INSTITUTE OF PHYSICS PUBLISHING JOURNAL OF MICROMECHANICS AND MICROENGINEERING

J. Micromech. Microeng. **14** (2004) 235–241 PII: S0960-1317(04)62475-2

The BELST II process for a silicon high-aspect-ratio micromaching vertical comb actuator and its applications

Julius Ming-Lin Tsai, Huai-Yuan Chu, Jerwei Hsieh and Weileun Fang

Power Mechanical Engineering Department, National Tsing Hua University, Hsinchu 30043, Taiwan

E-mail: fang@pme.nthu.edu.tw

Received 23 April 2003, in final form 3 October 2003
Published 17 November 2003
Online at stacks.iop.org/JMM/14/235 (DOI: 10.1088/0960-1317/14/2/010)

Abstract
The BELST process has been proposed and it has demonstrated the capability to overcome anchoring and depth controlling issues in many high-aspect-ratio micromaching (HARM) processes. However, the actuation mechanisms are still restricted to in-plane motion only. In this study, a novel fabrication process called BELST II has successfully been developed. Moreover, the BELST II process was employed to fabricate a novel electrostatic vertical comb actuator (VCA). Three advantages for this VCA can be observed. First, through some exquisite designs the fabrication process has no critical alignment and bonding problems. Secondly, the relative vertical position between the moving and the stationary fingers can be adjusted freely to optimize the performance of the VCA. Thirdly, both a large mirror structure and trimmed torsional spring are available through this process. Thus, improved performance regarding enlarged traveling distance with reduced driving voltage can be obtained. In the application of the BELST II process, various HARM devices were realized, such as an optical scanner mirror and variable optical attenuator driven by the VCA.

1. Introduction

The out-of-plane angular motion plays a crucial role in micromachined optical devices such as optical switches [1, 2] and optical scanners [3, 4]. The out-of-plane angular motion can be generated using different actuators, for instance, the gap closing actuator, scratch-drive actuator, and the linear comb actuator. The performance of these devices is limited to the linear operating range and, in addition, a complicated mechanism is required to transfer the in-plane motion to out-of-plane motion. Moreover, another consideration during design is to obtain a larger deflection angle as well as smaller driving voltage. The vertical comb actuator (VCA) is regarded as one of the most promising approaches to provide large out-of-plane angular motion. The VCA has been realized using various approaches, for instance, the silicon-on-insulator (SOI) technique [5], the bonding approach [6], and surface/bulk micromachining (SBM) technology [7]. High-aspect-ratio micromachining (HARM) processes have demonstrated their importance by offering even larger angular motion as well as extremely large and stiff microstructures [8–10]. However, these approaches may suffer from complex fabrication procedures, which induce the alignment and gap-expending problems.

Due to good mechanical isotropy [11], simple process steps, and low wafer cost, the fabrication of HARM structures on (111) single-crystal silicon wafers has been studied extensively [7, 12–14]. In addition, the lateral-silicon-etching mechanism allows the fabrication of a thick, suspended structure with an even surface on the (111) wafer. A novel 'boron etch-stop assisted lateral silicon etching'(BELST) process on the (111) wafer has been presented in [15]. The restrictions in the HARM process, including structure thickness/width limitation, anchor induced design problem, thickness uniformity, and sidewall conductivity problem, can all be reduced using the BELST process. However, the structures fabricated using the BELST process have uniform thickness, and thus their motion in the in-plane direction is

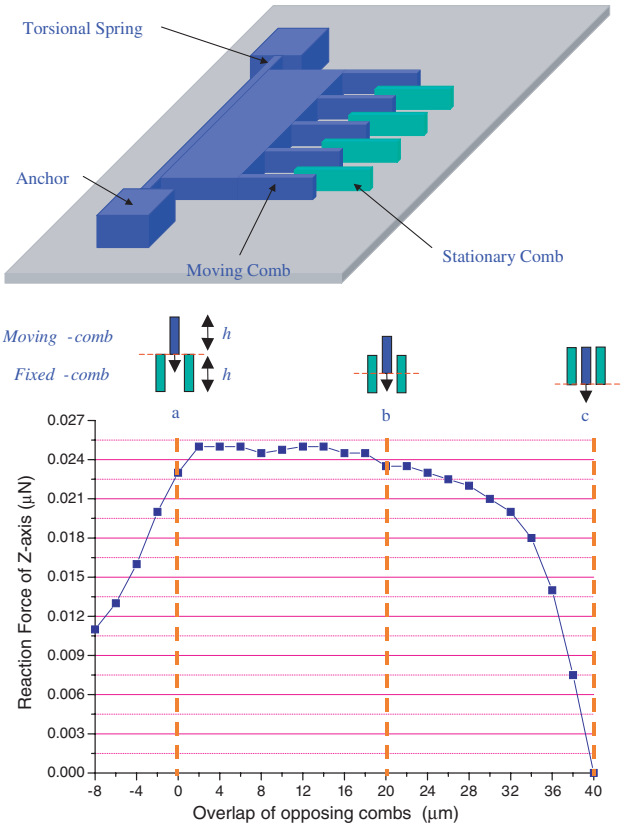

Figure 1. The predicted electrostatic force in the vertical direction as a function of the engagement of the comb electrodes (comb thickness is 40 μm).

restricted. To enable the out-of-plane motion, the extended BELST process has been proposed [16, 17]. Based on the BELST process with some added steps and layout design, VCAs can be realized within three masks.

In this paper, we rename the extended BELST process the BELST II process, to distinguish it from the BELST process that is only suitable for fabricating in-plane motion devices. The BELST II process has demonstrated the possibility of fabricating HARM VCAs on (111) silicon wafers without expending finger gaps or increasing process complexity. More detailed design issues, including HARM device fabrication with different thickness, height-difference generation of VCA, and layout design for better structure release, will be addressed in this paper. Furthermore, two micromachined optical devices driven by a VCA will be presented.

2. Design and analysis

In general, the VCA consists of comb fingers and torsional suspension, as shown in the upper part of figure 1. To figure out the best design value for the 'initial' overlap of opposing combs, MEMCAD [18] simulation for force values at different initial overlaps was performed. The typical result is shown in the lower part of figure 1, where the sizes for the VCA were set to 40 μm in finger thickness, 5 μm in finger width, and 4 μm in air gap. The electrostatic force approaches its maximum at the position where the moving comb finger initially overlaps with the stationary comb fingers (i.e., position 'a' indicated

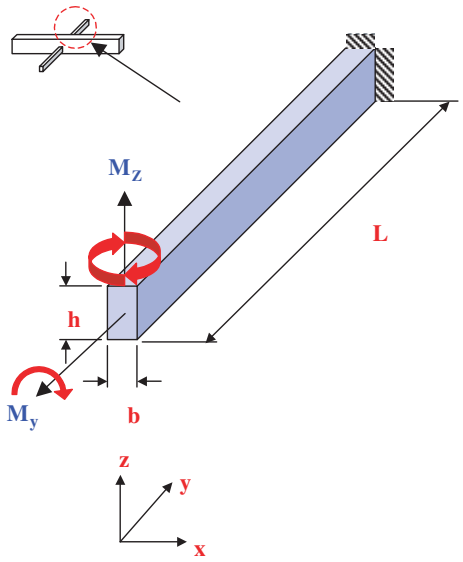

Figure 2. Schematic illustration of the torsional suspension.

in figure 1). The force is almost constant for the overlap between regions from 'a' to 'b', where 'b' represents overlap at half the thickness of the fingers. For the overlap larger than half the finger thickness, the force promptly drops to zero. The simulation results agree with the predictions in [19]. Accordingly, the initial force is highly dependent on the initial overlap of the opposing combs. In order to meet the operating requirements of the VCA for different applications, the initial overlap between moving and stationary comb fingers should be adjustable. Meanwhile, larger comb finger thickness is another consideration to enlarge the operating region of the VCA.

To guarantee the VCA with pure out-of-plane angular motion, the side sticking effect must be suppressed. To this end, it is necessary to have precise alignment between moving and stationary combs, i.e., patterning both combs in one mask. Besides, the suspension shown in figure 2 should have much larger torsional stiffness along the z-axis (in-plane direction) k_z than the y-axis (out-of-plane direction) k_y. As shown in figure 2, the out-of-plane torsional stiffness k_y of the HARM suspension (thickness > width) of thickness h, width b, and length L can be expressed as [20]

$$k_y = \frac{Ghb^3}{16L}\left[\frac{16}{3} - 3.36\frac{b}{h}\left(1 - \frac{1}{12}\frac{b^4}{h^4}\right)\right] \tag{1}$$

where G is the shear modulus of the material. In addition, the in-plane torsional stiffness k_z of the suspension can be expressed as [20]

$$k_z = \frac{2Ehb^3}{3L} \tag{2}$$

where E is the Young's modulus of the material. The stiffness ratio K, which is the ratio of out-of-plane stiffness k_y to the in-plane stiffness k_z, can be expressed as

$$K = \frac{G}{E}\left[\frac{1}{2} - 0.32\frac{b}{h}\left(1 - \frac{1}{12}\frac{b^4}{h^4}\right)\right]. \tag{3}$$

Since the parameters G and E are material constants, the stiffness ratio K is only determined by the aspect ratio b/h. The out-of-plane torsional stiffness k_y of the suspension should

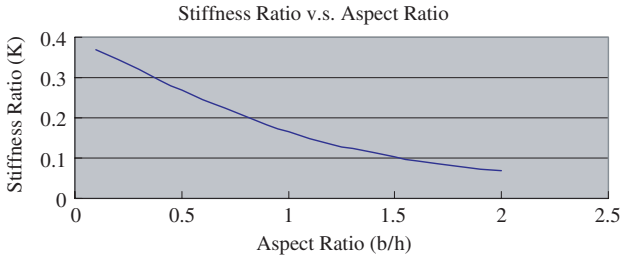

Figure 3. Comparison of stiffness ratio between out-of-plane axis torsion and in-plane axis twisting.

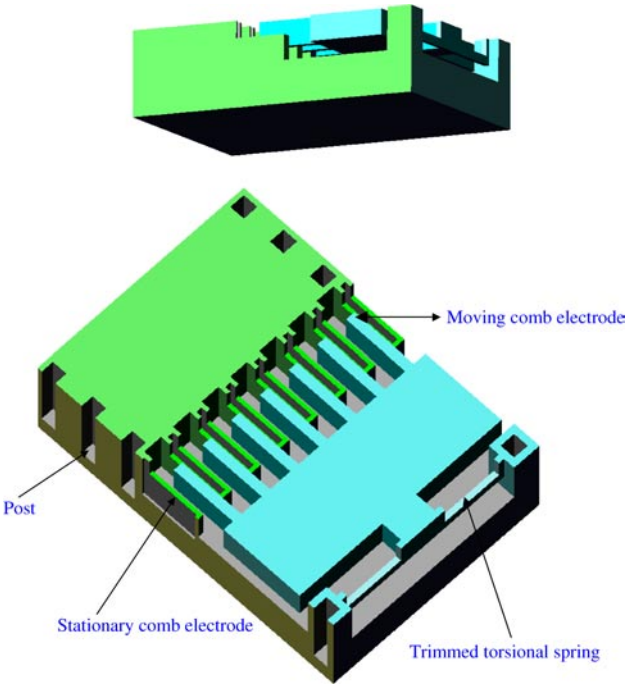

Figure 4. Proposed design of the VCA.

be reduced to lower the driving voltage, whereas the in-plane torsional stiffness k_z of the suspension should be increased to prevent side sticking. In other words, a smaller stiffness ratio K is preferred in this design. Figure 3 shows the variation of the stiffness ratio K with the aspect ratio b/h. It is evident that a suspension with larger aspect ratio b/h is required to prevent the VCA from side sticking. Thus, a smaller suspension thickness h is preferred. To this end, the fabrication process must have the ability to selectively trim the spring thickness while the comb thickness remains unchanged to meet the thick-comb requirement for the VCA.

The expected HARM VCA design is schematically illustrated in figure 4. This device can meet two critical design issues to improve the performance of the VCA. The first consideration is the relative position of the stationary and moving electrodes. As indicated in figure 4, the height of the stationary comb electrodes needs to be trimmed. Secondly, the thickness of the suspension should be smaller than that of the electrodes to decrease the driving voltage of the VCA. In this regard, the thickness of the torsional suspension also needs to be trimmed. To demonstrate the feasibility of the BELST II process, the VCA in figure 4 has been fabricated.

3. Fabrication and results

In this section, we present the BELST II process. The BELST II process is a modification of the BELST process, and applicable to (111) silicon substrate [15]. Accordingly, various merits in the BELST process have been employed in the BELST II process, such as using the guarding wall to control structure thickness and the boron etch-stop (BES) post to firmly establish strong anchors. Three advantages can be observed, including its non-complex process that has no critical alignment problem [7, 21]: adjustable comb relative position, available large mirror structure and trimmed torsional spring. Moreover, a new trimming process combining BES posts can not only extend the design of torsional bars but also provide a promising way to fabricate the VCA. In the application of the BELST II process, the VCA illustrated in figure 4 was fabricated and then tested.

The typical process steps for the BELST II process are shown in figure 5. This figure shows the process sequence to fabricate a HARM VCA. As shown in figure 5(a), the process began with boron diffusion on n-type (111) silicon wafer, followed by a thin silicon nitride (SiN_x) layer deposition. After this, the first SiO_2 layer was deposited by plasma enhanced chemical vapor deposition (PECVD) and patterned using buffered oxide etcher to serve as the trimming mask. This mask defined the structures to be trimmed including stationary comb electrodes and torsional suspensions as shown in figure 4. The second SiO_2 layer was then deposited on the substrate. Figure 5(b) shows that the unwanted SiN_x and SiO_2 layers were removed by the reactive ion etching (RIE) process. Thus, the planar shape of the VCA in figure 4 was defined. Since the moving and stationary comb fingers were patterned simultaneously in one mask, the misalignment problem was prevented and a small comb gap was achieved. As shown in figure 5(c), a thick photoresist (PR) layer was used to define locations of the BES post to anchor the stationary comb electrodes and bonding pads of the VCA. In summary, the processes in figures 5(a)–(c) were employed to deposit and pattern three etching masks.

After the etching masks were patterned, the depth of the BES post was defined by the first deep reactive ion etching (DRIE) process, as shown in figure 5(d). After stripping the PR layer, another DRIE shown in figure 5(e) was carried out to define the thickness of the VCA. The boron diffusion process in figure 5(f) was then conducted to provide sidewall boron diffusion. This boron-doped silicon was exploited not only to prevent the sidewall from etching in alkaline solution but also to serve as a conducting layer and p–n–p junction isolation. Figure 5(g) shows that the VCA was selectively trimmed using the third DRIE, and hence the height of the stationary electrodes was tuned to offer a better initial engagement between the electrodes. Moreover, the thickness of the torsion suspension was decreased in this step to reduce the driving voltage. However, a thick and stiff structure, such as a mirror, was still available. Finally, the VCA was released into alkaline solution after an anisotropic lateral etching, as shown in figure 5(h). In short, one wet etching and three DRIE processes were employed in figures 5(d)–(h) to fabricate three-dimensional HARM structures with various thicknesses. In addition, the bonding process was not required.

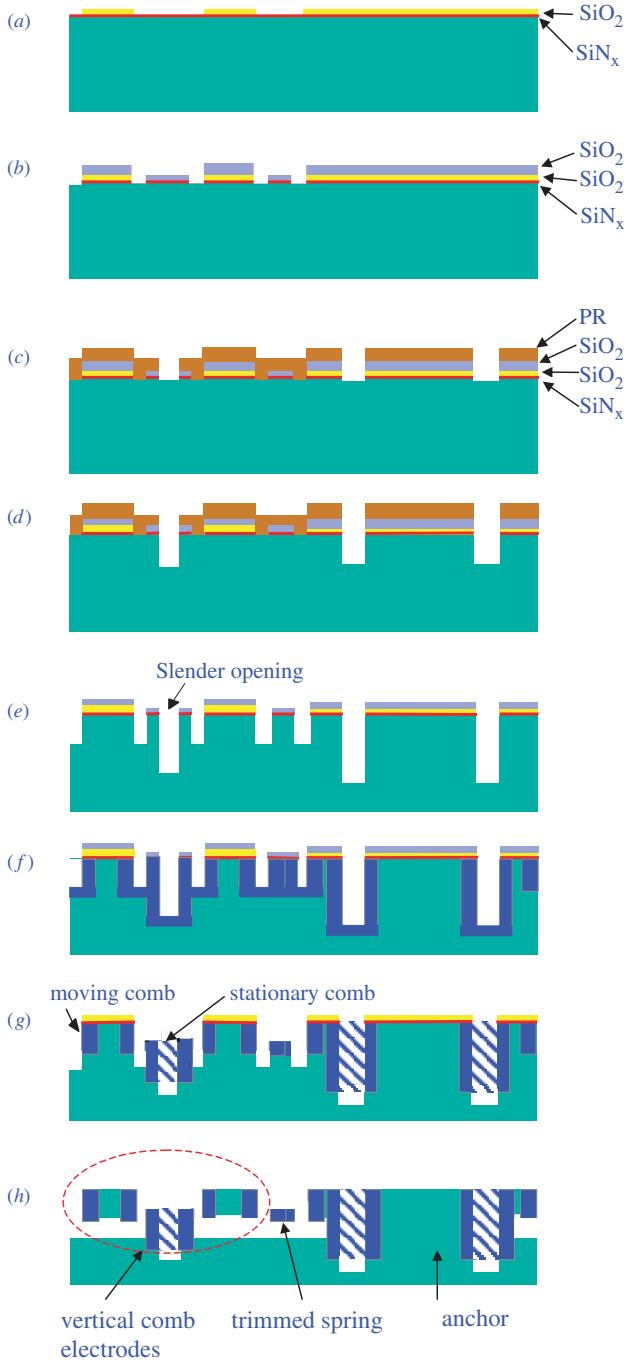

Figure 5. Fabrication sequence for the BELST II process (*a*) define trim area, (*b*) define structure, (*c*) define POST, (*d*) 1st DRIE, (*e*) 2nd DRIE, and remove PR, (*f*) boron diffusion, (*g*) remove SiO_2, and 3rd DRIE and (*h*) laterally releasing, and remove SiN_x.

The releasing mechanism is different between (100) and (111) silicon substrates. The hexagonal cavity shown in figure 6 is formed by (111) sidewalls after undercutting an opening on (111) silicon substrate. To establish a firm anchor, the BES posts should be placed at the convex corner of the hexagon that has been exploited in [1]. However, to release a large area of a structure such as a mirror, the releasing holes, as used in surface micromachining, have no effect at all. The holes should be replaced by a long and slim

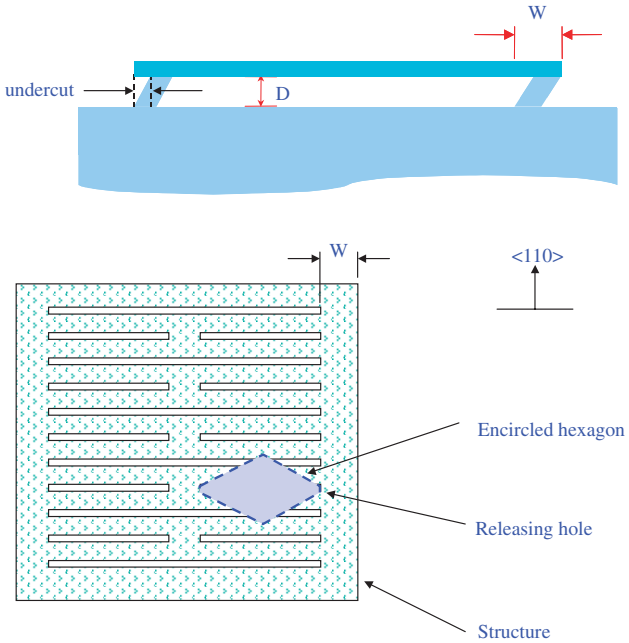

Figure 6. Schematic illustrations of the releasing stripes and encircled hexagon.

stripe. If the distance between the openings is small enough, the adjacent hexagonal cavities will form convex corners. Thus, the undercut process can be continued, and most of the structure can be released. This effect has been used to reduce the etching time while releasing a large area structure such as a mirror. However, the regions ($W \times L$) at both sides of the structure cannot be undercut using this approach. In this regard, the criteria $W \leqslant D \times Cot(70.53^\circ)$ must be fulfilled to release this region, where D is the thickness of the substrate to be removed, as shown in figure 6.

Figure 7 shows scanning electron microscopy (SEM) micrographs of the fabricated VCA. As indicated in figure 7(*a*), the hollow stationary comb finger is anchored to the substrate at the center by the BES post. Figure 7(*b*) shows the initial engagement between the trimmed stationary and moving comb fingers. These results demonstrate that the operating region of the VCA can be tuned by the thickness trimming process of BELST II. The photograph in figure 8 shows the torsional spring of the mirror. From the higher-magnification micrograph, the trimming of the spring thickness can be clearly seen. In the experiment, the thickness h of the torsional spring was trimmed to range from 25 to 8 μm. Since the width b of the torsional spring was 8 μm, the aspect ratio b/h was tuned to range from 0.32 to 1. According to the theoretical predication in figure 3, the stiffness ratio K decreased from 0.31 to 0.16. The trimmed torsional spring reveals the capability of realizing a three-dimensional HARM structure using the BELST II process, which can further reduce driving voltage yet prevent the device from side sticking. Since the thickness of the mirror plate was not trimmed, the mirror had a large stiffness and its radius of curvature was around tens to a hundred millimeters. In addition, the surface roughness of the mirror was below 40 nm.

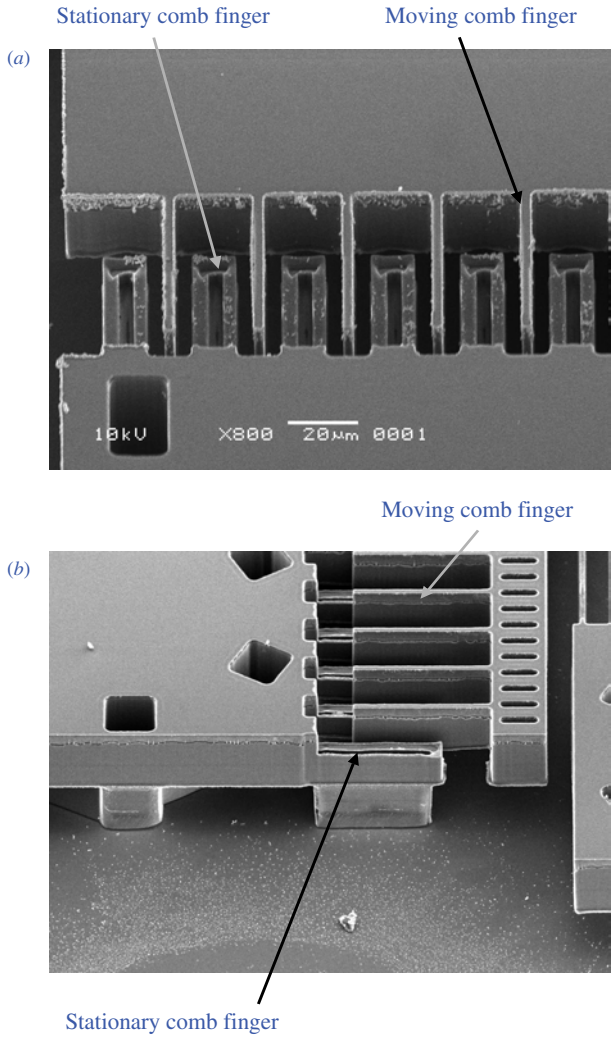

Figure 7. SEM micrographs showing the stationary and moving comb electrodes of the fabricated VCA: (*a*) top view; (*b*) side view. The initial engagement of the comb electrodes can be observed from the side view.

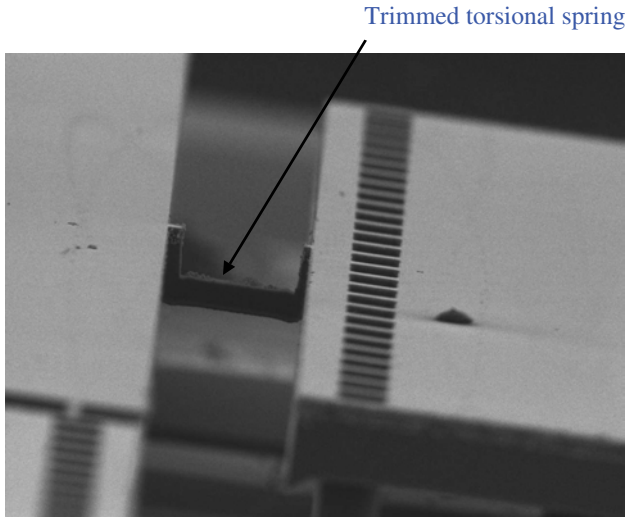

Figure 8. SEM micrograph showing the trimmed torsional suspension of the VCA.

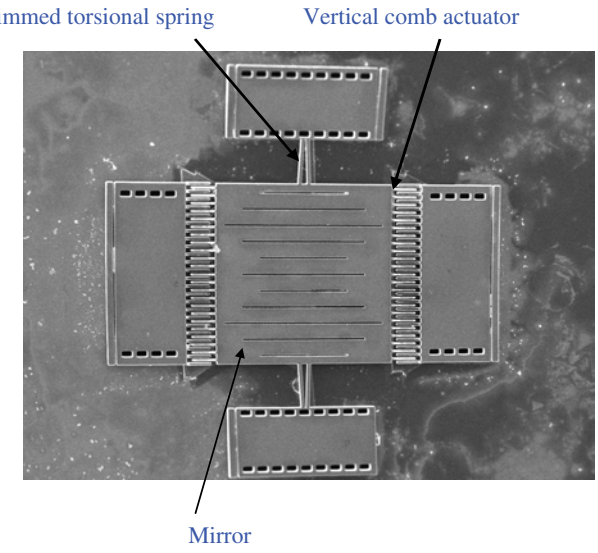

Figure 9. SEM micrograph showing the fabricated optical scanner driven by the VCA.

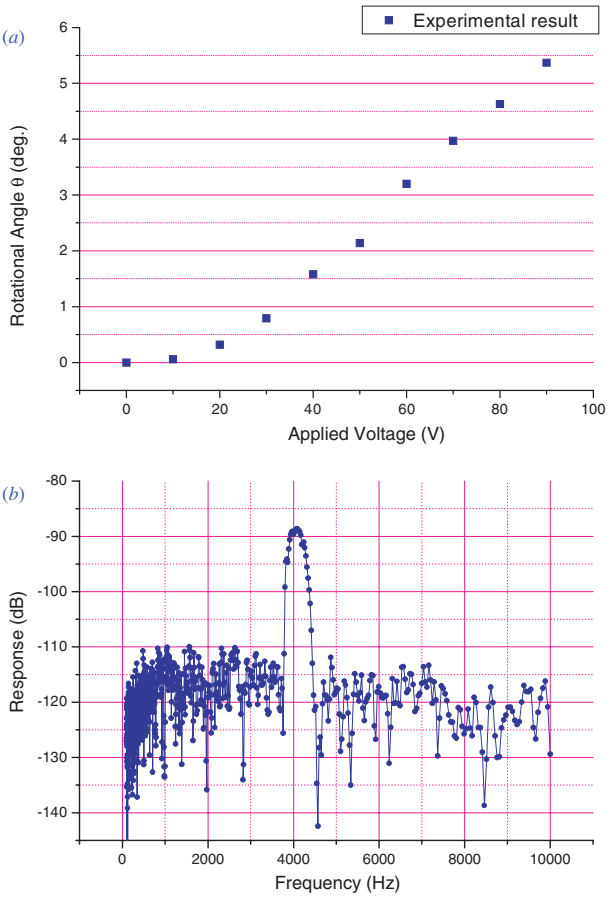

Figure 10. (*a*) Static and (*b*) dynamic performance of the optical scanner.

4. Applications

As the first application, the optical scanner driven by the VCA was designed and fabricated in this study, as shown in figure 9. By using stripe-type etching holes, a mirror

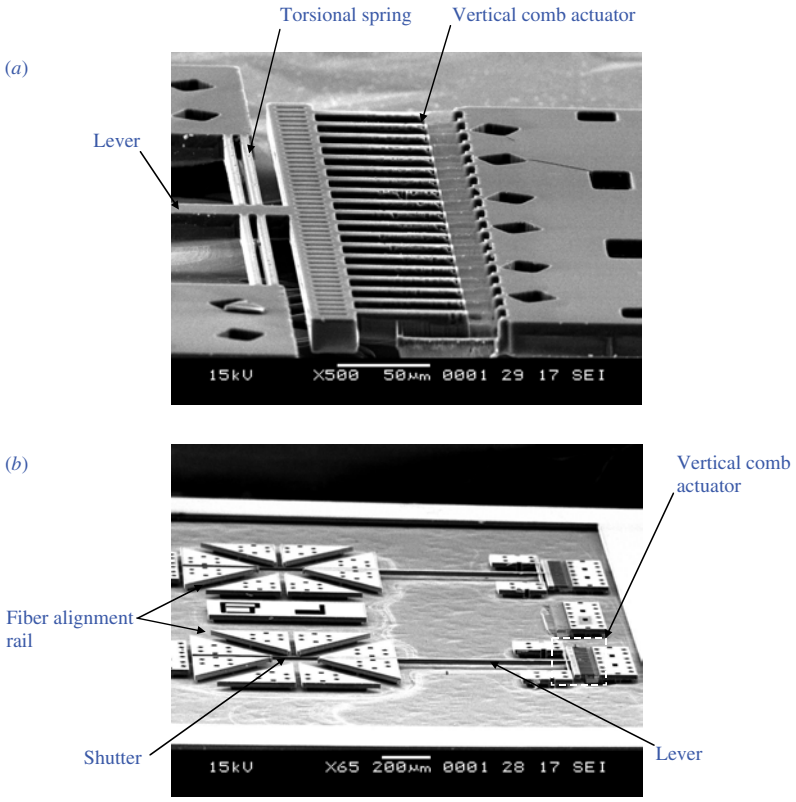

Figure 11. SEM micrographs showing (*a*) the combination of VCA and leverage was devised to amplify the out-of-plane motion of the shutter, and (*b*) the fabricated 2 × 2 optical switch. The fiber alignment rail was also available using the BELST II process.

with an area of 500 × 500 μm^2 can be released. With VCAs at both sides, the mirror can be operated linearly by applying push–pull voltage. The static characteristics of the optical scanner driven by the VCA with direct-current (dc) voltage were measured by optical interferometer. The typical measured load–deflection relation of the torsional micromirror is depicted in figure 10(*a*). This demonstrates that the torsional micromirror has an optical scanning angle near 5° when driven at 90 V. Various optical scanners driven by the VCA have been reported in [4, 21–25]. By way of comparison with a typical scanner fabricated using a SOI wafer [22], the optical scanning angle was near 4° when driven at 80 V. Note that no side-sticking phenomenon was observed during the driving test. From figure 10(*a*) we can find that when the deflection angle is larger than 3°, the variation of the angle with the driving voltage no longer follows the quadratic relationship predicted from analysis. One of the possible reasons is that the VCA has reached its half-engagement, where its electrostatic force begins to decrease as comb engagement increases. This can further be improved by making the VCA with larger position-independent range using the BELST process. Another reason may come from the sidewall shrinkage of the stationary finger due to the limited etch-stop ability of boron diffusion. Increasing the doping time can also improve this situation. Moreover, the dynamic characteristics of the VCA driven by alternating current (ac) voltage were measured by laser Doppler vibrometry. Figure 10(*b*) shows the frequency response of the VCA when applying 20 V_{pp}. The peak at 4.1 kHz with a quality factor of 7 results from the resonance of the structure, and the associated optical scanning angle was 35°. As a comparison, the optical scanning angle was 25° in [4]. In [4], additional wafer bonding and back-side deep etching processes were required to fabricate the scanner. This demonstrates that the proposed VCA has a low driving voltage and a large angular displacement.

Another potential optical application of the VCA using the BELST II process is demonstrated in figure 11. As shown in figure 11(*a*), the combination of VCA and leverage was devised to amplify the out-of-plane motion of the shutter, so as to reflect or obstruct the light beam coming from the optical fibers. The preliminary experimental results have shown that the tip deflection of the shutter was more than 10 μm and its resonant frequency ranged from 2 to 5 kHz. As shown in figure 11(*b*), the fiber alignment rail was also available using the BELST II process, and hence the 2 × 2 optical switch and variable optical attenuator were realized. In conclusion, various HARM devices driven by the VCA can also be realized by the BELST II process.

Acknowledgments

This research is based on the work supported by WALSIN LIHWA Corporation and the Ministry of Economic Affairs, Republic of China under contract no 91-EC-17-A-07-S1-0011. The authors would like to thank the Central Regional MEMS Research Center of the National Science Council, Semiconductor Research Center of National Chiao Tung University and National Nano Device Laboratory for providing the fabrication facilities.

References

[1] Lee S, Huang L S, Kim C and Wu M C 1999 Free-space fiber-optic switches based on MEMS vertical torsion mirrors *J. Lightwave Technol.* **17** 7–13

[2] Lin L Y and Goldstein E L 1999 Micro-electro-mechanical systems (MEMS) for WDM optical-crossconnect networks *MILCOM 1999 (Atlantic City, NJ, Oct. 1999)* vol 2 pp 954–7

[3] Kiang M, Solgaard O, Muller R S and Lau K Y 1996 Surface-micromachined electrostatic-comb driven scanning micromirrors for barcode scanners *MEMS'96 (San Diego, CA, Feb. 1996)* pp 192–7

[4] Conant R A, Nee J T, Lau K Y and Muller R S 2000 A flat high-frequency scanning micromirror *Proc. 2000 Solid-State Sensor and Actuator Workshop (Hilton Head Island, SC, June 2000)* pp 6–9

[5] Yeh J A, Jiang H and Tien N C 1999 Integrated polysilicon and DRIE bulk silicon micromachining for an electrostatic torsional actuator *J. Microelectromech. Syst.* **8** 456–65

[6] Kim J, Ko Y, Kong D, Lee K B and Jeon D 2000 Fabrication of silicon optical scanner for laser display *IEEE/LEOS Int. Conf. on Optical MEMS (NJ)* pp 13–4

[7] Kim J, Park S and Cho D 2001 A novel electrostatic vertical actuator fabricated in one homogeneous silicon wafer using extended SBM technology *Transducers'01 (Munich, June 2001)* vol 1 pp 756–9

[8] Shaw K A, Chang Z L and MacDonald N C 1994 SCREAM I: a single mask, single-crystal silicon, reactive ion etching process for microelectromechanical structures *Sensors Actuators* A **40** 210–3

[9] Klaassen E H, Petersen K E, Noworolski J M, Logan J, Maluf N I, Brown J, Storment C, McCullcy W and Kovacs G T A 1995 Silicon fusion bonding and deep reactive ion etching a new technology for microstructures *Transducers'95/Eurosensors IX (Stockholm, Sweden, June 1995)* pp 556–9

[10] Gianchandani Y and Najafi K 1992 A bulk silicon dissolved wafer process for microelectromechanical devices *J. Microelectromech. Syst.* **1** 77–85

[11] Peterson K E 1982 Silicon as mechanical material *Proc. IEEE* **70** 420–57

[12] Fleming J G 1998 Combining the best of bulk and surface micromachining using Si {111} substrate *Proc. SPIE (Santa Clara, CA, Sept. 1998)* vol 3511 pp 162–8

[13] Chou B C S, Chen C N and Shie J S 1999 Micromachining on (111)-oriented silicon *Sensors Actuator* A **75** 271–7

[14] Oosterbroek R E, Berenschot J W, Jansen H V, Nijdam A J, Pandraud G, van den Berg A and Elwenspoek M C 2000 Etching methodologies in <111>-oriented silicon wafers *J. Microelectromech. Syst.* **9** 390–8

[15] Hsieh J and Fang W 2002 A boron etch-stop assisted lateral silicon etching process for improved high-aspect-ratio silicon micromachining and its applications *J. Micromech. Microeng.* **12** 574–81

[16] Hsieh J, Chu C C, Tsai J M and Fang W 2002 Using extended BELST process in fabricating vertical comb actuator for optical applications *IEEE/LEOS Int. Conf. on Optical MEMS (Lugano, Switzerland, Aug. 2002)* Paper WP 39

[17] Chu C C, Tsai J M, Hsieh J and Fang W 2003 A novel electrostatic vertical comb actuator fabricated on (111) silicon wafer *IEEE MEMS'03 (Kyoto, Japan, Jan. 2003)* pp 56–9

[18] http://www.coventor.com/

[19] Yeh J A, Hui C-Y and Tien N C 2000 Electrostatic model for an asymmetric combdrive *J. Microelectromech. Syst.* **9** 126–35

[20] Roark R J 1965 *Formulas for Stress and Strain* 4th edn (New York: McGraw-Hill)

[21] Patterson P R, Hah D, Nguyen H, Toshiyoshi H, Chao R M and Wu M C 2002 A scanning micromirror with angular comb drive actuation *IEEE MEMS'02 (Las Vegas, NV, Jan. 2002)* pp 544–7

[22] Overstolz T, Clerc P-A, Gale M T, Herzig H P, Niederer G, Noell W, Sochtig J, Thiele H and de Rooij N F 2002 Tilting out-of-plane platform for optical applications *IEEE Optical MEMS'02 (Lugano, Switzerland, Aug. 2002)* pp 81–2

[23] Lee J-H, Ko Y-H, Choi B-S, Kim J-M and Jeon D-Y 2002 Bonding of silicon scanning mirror having vertical comb fingers *J. Micromech. Microeng.* **12** 644–9

[24] Kwon S, Milanovic V and Lee L P 2002 Large-displacement vertical microlens scanner with low driving voltage *IEEE Photon. Technol. Lett.* **14** 1572–4

[25] Milanovic V, Matus G A, Cheng T and Cagdaser B 2003 Monolithic high aspect ratio two-axis optical scanners in SOI *IEEE MEMS'03 (Kyoto, Japan, Jan. 2003)* pp 255–8